

THERMAL PROPERTIES AND HOMOGENITY RANGE OF $\text{Bi}_{24+x}\text{Co}_{2-x}\text{O}_{39}$ CERAMICS

[#]O. JANKOVSKY*, D. SEDMIDUBSKY*, Z. SOFER*, J. CAPEK**, K. RUZICKA***

*Department of Inorganic Chemistry, Institute of Chemical Technology Prague,
Technická 5, 166 28 Prague 6, Czech Republic

**Department of Metals and Corrosion engineering, Institute of Chemical Technology Prague,
Technická 5, 166 28 Prague 6, Czech Republic

***Department of Physical Chemistry, Institute of Chemical Technology Prague,
Technická 5, 166 28 Prague 6, Czech Republic

[#]E-mail: Ondrej.Jankovsky@vscht.cz

Submitted February 25, 2013; May 7, 2013

Keywords: Cobalt sillenite, Thermal properties, Heat capacity

Samples with different $\text{Bi}_2\text{O}_3/\text{Co}_2\text{O}_3$ ratio were prepared by ceramic route. Based on the results of DTA, XRD and SEM – EDX a section of phase diagram of the Bi–Co–O diagram in air atmosphere was calculated using the FactSage software. The sillenite structure of $\text{Bi}_{24+x}\text{Co}_{2-x}\text{O}_{39}$ was confirmed and described. The Rietveld analysis confirmed SEM – EDX results. The heat capacity and enthalpy increments of $\text{Bi}_{24}\text{Co}_2\text{O}_{39}$ were measured by differential scanning calorimetry (DSC) from 258 K to 355 K and by the drop calorimetry from 573 K to 973 K. Above room temperature the temperature dependence of the molar heat capacity in the form $C_{pm} = (1467.87 + 0.299410 \cdot T - 15888378 \cdot T^2) \text{ J K}^{-1} \text{ mol}^{-1}$ was derived by least-squares method from the experimental data.

INTRODUCTION

Nowadays there are not many reports on high temperature phase relations in the Bi–Co–O system because bismuth and bismuth (III) oxide are very aggressive to all apparatus and laboratory equipment at elevated temperatures. The properties and structure polymorphs of bismuth sesquioxide were studied by Harwig [1]. The phase diagram of pseudobinary system Bi–Co–O at room temperature as a part of Bi–Co–Nb–O system was published in Vanderah's et al. work [2]. In this work the thermodynamic behavior of stoichiometric compound $\text{Bi}_{25}\text{CoO}_{40}$ is described. This compound represents in fact a Co rich end-member of a solid solution adopting the sillenite structure, which can be described as a stabilized $\gamma\text{-Bi}_2\text{O}_3$. The group of sillenites was discovered and described by Sillen et al. [3]

A number of various sillenite structures with a general formula $\text{Bi}_{24}\text{M}_2\text{O}_{40-6}$ has been synthesized so far. A stoichiometric model for sillenites was established by Valant et al. [4] who confirmed a formation of $\text{Bi}_{24}\text{M}^{n+}_{2-x}\text{O}_{40}$, where M^{n+} is Cd^{2+} , Zn^{2+} , Ga^{3+} , Fe^{3+} , Cr^{3+} , Tl^{3+} , Si^{4+} , Ti^{4+} , Ge^{4+} , Mn^{4+} , V^{5+} , As^{5+} and P^{5+} . The structure of $\text{Bi}_{12.7}\text{Co}_{0.3}\text{O}_{19.35}$ was reported by Mary et al. [5]. Applying hot pressing technique a perovskite type structure BiCoO_3 was stabilized at elevated pressures in the Belt-type apparatus [6].

In this study we investigated the homogeneity range and thermal properties of $\text{Bi}_{24+x}\text{Co}_{2-x}\text{O}_{39}$. The section of Bi–Co–O phase diagram was constructed using

FactSage software [7], where molar fraction of Co is between 0 and 0.15. The knowledge of heat capacity of $\text{Bi}_{24+x}\text{Co}_{2-x}\text{O}_{39}$ phase is important due to further calculations of phase equilibria in Bi–Sr–Co–O system which are currently in progress. The misfit layered cobaltite $[\text{Bi}_2\text{Sr}_2\text{O}_3][\text{CoO}_2]_{1.82}$ represents one of the ternary oxides occurring in the Bi–Sr–Co–O system and is well known as a p-type thermoelectric material. Misfit cobaltites such as $[\text{Bi}_2\text{Sr}_2\text{O}_3][\text{CoO}_2]_{1.82}$ and $[\text{Ca}_2\text{CoO}_3][\text{CoO}_2]_{1.62}$ can be used in high temperature thermoelectric batteries for energy recovery of the heat waste. [8–10]. Since $\text{Bi}_{24+x}\text{Co}_{2-x}\text{O}_{39}$ appears to be the only binary oxide stable in Bi–Co–O subsystem, we can expect its coexistence field with the misfit layer cobaltite, which might be of importance for the fabrication of thermoelectric materials with controlled microstructure.

EXPERIMENTAL

All samples were prepared by conventional ceramic route from pure Bi_2O_3 and Co_2O_3 powders. Precursors were mixed in stoichiometric rates 98/2 (B98C2), 97/3 (B97C3), 95/5 (B95C5), 92.3/7.7 (B24C2), 90/10 (B9C1) and 80/20 (B8C2) and homogenized in the agate mortar. Powders were then calcined in the platinum crucible at 973 K for 24 hours, once more homogenized and calcined at 1003 K for the next 24 hours. After manual homogenization, all samples were cold pressed under pressure of 0.5 GPa. Pellets were sintered for

200 hours in air atmosphere at 1013 K and they were cooled down with cooling rate 1 K/min to room temperature.

All samples were analyzed by X-Ray powder diffraction (XRD) on *Bruker AXS D8* θ - θ powder diffractometer with parafocusing Bragg–Brentano geometry using CoK_α radiation ($\lambda = 1.79021 \text{ \AA}$, $U = 34 \text{ kV}$, $I = 20 \text{ mA}$). To confirm the composition of the phase diagram at 973 K a number of high-temperature annealing experiments at 973 K was performed followed by rapid quenching to room temperature. Samples were thrown into a container with liquid nitrogen. Such a rapid cooling is expected to quench the high temperature thermodynamic equilibrium state. All quenched samples were analyzed by XRD. Powder diffraction data were analyzed by *HighScore Plus* software and by Rietveld analysis using *FullProff* software to specify phase composition and lattice parameters of $\text{Bi}_{24+x}\text{Co}_{2-x}\text{O}_{39}$ phase.

Samples were analyzed by energy-dispersive X-ray spectroscopy (SEM-EDX) on *TESCAN Vega 3 LMU* microscope with *Oxford instruments INCA 350 EDS analyser* to confirm the Rietveld analysis results. Thermal analysis was measured by differential thermal analysis (DTA) and thermogravimetry (TG) from 293 K to 1200 K to determine melting temperature of $\text{Bi}_{24+x}\text{Co}_{2-x}\text{O}_{39}$ system. DTA and TG curves were measured simultaneously on *Setaram STA* apparatus model *Setsys Evolution* with a heating rate 10 K/min.

The measurements of heat capacity were performed on the sample B24C2 by a similar method and instrumentation as described by Leitner et al. [11]. A *Micro DSC III* calorimeter (Setaram, France) was used for the heat capacity determination in the temperature range of 258 – 355 K. The heat capacity was measured in the incremental temperature scanning mode consisting of a number of 5 K steps (heating rate 0.3 K min^{-1}) followed by the isothermal delays of 2600 s. Two subsequent step-by-step heating were recorded. Synthetic sapphire, NIST Standard reference material No. 720, was used as the reference. The uncertainty of heat capacity measurements is estimated to be better than $\pm 1 \%$.

Enthalpy increment determinations were carried out by drop method using high temperature calorimeter *Multi HTC 96* (Setaram, France). All measurements were performed in air by the alternating dropping of a reference material (small pieces of synthetic sapphire, NIST Standard reference material No. 720) and of a sample (small pieces of pallets) being initially held at room temperature, through a lock into the working cell of the preheated calorimeter in a following sequence: standard – sample – standard – sample – standard. Endothermic effects are detected and the relevant peak area is proportional to the heat content of the dropped specimen. The measurements were performed at temperatures 573 K to 973 K on samples of 300 - 400 mg, which provide similar thermal effect as standards. The delays

between two subsequent drops were 20 min to stabilize heat flow. To check the accuracy of measurement, the enthalpy increments of platinum in the temperature range 770 – 1370 K were measured first and compared with published reference values [12]. The average relative error was under 1%. Estimated overall accuracy of the drop measurements is $\pm 3\%$.

The phase equilibria calculation and the construction of the phase diagram section was performed by the *FactSage* thermochemical software. The sublattice model was used for thermodynamic description of $\text{Bi}_{24+x}\text{Co}_{2-x}\text{O}_{39}$ and stoichiometric phases $\gamma\text{-Bi}_2\text{O}_3$ and $\text{Bi}_{24}\text{Co}_2\text{O}_{39}$ were considered as the end-members [13]. Standard enthalpies of formation and entropies referred to ambient temperature ($T = 298 \text{ K}$) and on the temperature dependence of heat capacity in a polynomial form were used for calculation of Gibbs energies. These values are stored in *FactSage* compound database format. All values were set identically to work [13] apart from the dependence of heat capacity of the end-member $\text{Bi}_{24}\text{Co}_2\text{O}_{39}$, which was determined from heat capacity and relative enthalpy measurements obtained in this study.

RESULTS AND DISCUSSION

XRD analysis showed the presence of three different phases at ambient temperature in this system. Bi-rich samples contained $\alpha\text{-Bi}_2\text{O}_3$ and $\text{Bi}_{24+x}\text{Co}_{2-x}\text{O}_{39}$ phase. Samples B95C5 and B24C2 were single phase and contained only $\text{Bi}_{24+x}\text{Co}_{2-x}\text{O}_{39}$ phase. Co-rich samples contained a mixture of $\text{Bi}_{24+x}\text{Co}_{2-x}\text{O}_{39}$ and Co_3O_4 spinel phase (see Figure 1). Surprisingly, XRD analysis of rapidly quenched samples showed presence of the same phases in almost the same ratio. These results were confirmed by SEM-EDX, although higher miscibility on both sides of $\text{Bi}_{24+x}\text{Co}_{2-x}\text{O}_{39}$ was expected at elevated

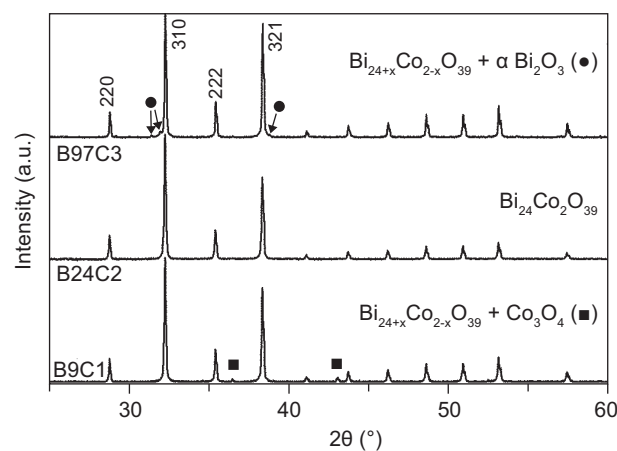


Figure 1. XRD of three samples in Bi–Co–O system. B24C2 contains only one phase, while B97C3 and B9C1 are two-phase.

temperatures. Accordingly the Co-substitution on the Bi-sublattice is obviously energetically unfavorable and there is also a considerable and steep departure from ideal mixing on Co-sublattice, which avoid opening of broader homogeneity range in $\text{Bi}_{24+x}\text{Co}_{2-x}\text{O}_{39}$.

Rietveld analysis of two-phase slowly cooled samples was made to determine the single phase homogeneity range of $\text{Bi}_{24+x}\text{Co}_{2-x}\text{O}_{39}$ solid solution. The value of x values ranging from ~ 0 to ~ 1 was obtained from both the phase ratio and from the refined Bi/Co ratio on Co-sublattice. The same approach was applied to the rapidly quenched samples to determine the single phase homogeneity range of $\text{Bi}_{24+x}\text{Co}_{2-x}\text{O}_{39}$ phase at 973 K. SEM-EDX analysis confirmed the results obtained by Rietveld analysis.

By means of DTA, the eutectic melting temperature of $\text{Bi}_{24}\text{Co}_2\text{O}_{39}$ composition was determined at 1036 K. In fact, this composition is out of the single-phase homogeneity range and, according to the thermodynamic model, this sample also contains a small amount of Co_3O_4 ; however, this amount cannot be detected. This value is in agreement with other DTA measurements in Co-rich region. The second eutectic point at 1039 K was determined in Bi-rich region. The solid state transition at 1015 K was obtained for sample B95C5.

The oxygen non-stoichiometry of $\text{Bi}_{24}\text{Co}_2\text{O}_{39}$ was measured by thermogravimetric analysis. The overall weight loss of 0.15 % (referred to the original sample mass) was found during the heating from the ambient temperature to the melting temperature. Furthermore the sample lost an additional weight of 0.07 % during the melting process. We assume that all the weight loss is caused by oxygen release (see Figure 2). This amount corresponds to the $\text{Bi}_{24}\text{Co}_2\text{O}_{38.25}$ stoichiometry at 1035 K before the decomposition and to the $\text{Bi}_{24}\text{Co}_2\text{O}_{38.8}$ at ambient temperature if we assume an ideal model of oxide melt based on the presence of Co^{2+} and Bi^{3+} cations. If the melt does not behave ideally and a fraction of cobalt is in Co^{3+} state, then the overall oxygen stoichiometry can

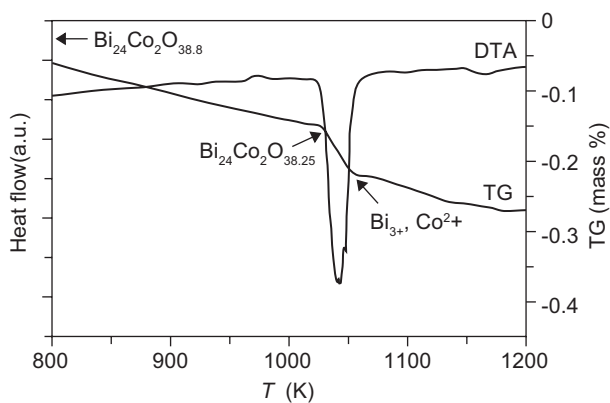


Figure 2. DTA and TG curves of $\text{Bi}_{24}\text{Co}_2\text{O}_{39}$ in purified air atmosphere ($p_{\text{O}_2}/p^0 = 0.21$, where $p^0 = 101.3$ kPa) with figured oxygen non-stoichiometry. The only one visible effect is the melting temperature.

be even higher than $\text{Bi}_{24}\text{Co}_2\text{O}_{38.8}$ at ambient temperature. The measured data used for further analysis of heat capacity involve 38 points from DSC (258 - 355 K) and 10 values of the enthalpy increments from the drop measurements (573 - 973 K). All C_{pm} data are plotted in Figure 3 and the enthalpy increment data are shown in Figure 4. For the assessment of the C_{pm} temperature dependences above room temperature, the heat capacity data from DSC and the enthalpy increment data from drop calorimetry were treated simultaneously by the linear least-squares method (Fit). This procedure was described in detail by Leitner et al. [11]. The temperature dependence of C_{pm} was considered in the form:

$$C_{pm} = A + B \cdot T + C \cdot T^2 \quad (1)$$

thus the related temperature dependence of $\Delta H_m(T) = H_m(T) - H_m(T_0)$ is given by equation:

$$\Delta H(T) = H(T) - H(T_0) = A \cdot (T - T_0) + \frac{1}{2} B \cdot (T^2 - T_0^2) - C \cdot \left(\frac{1}{T} - \frac{1}{T_0} \right) \quad (2)$$

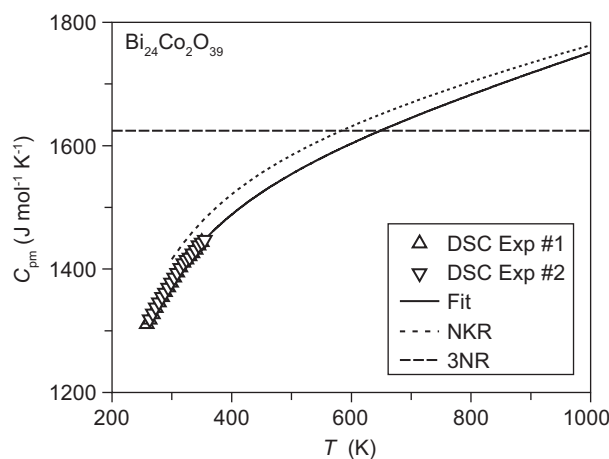


Figure 3. Heat capacity of $\text{Bi}_{24}\text{Co}_2\text{O}_{39}$. Experimental data were measured by DSC.

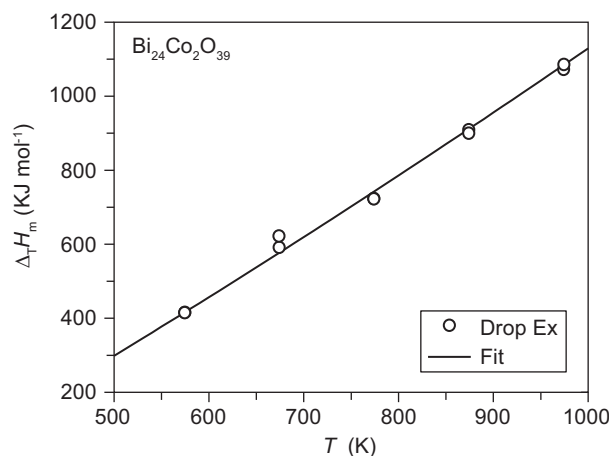


Figure 4. Enthalpy increments of $\text{Bi}_{24}\text{Co}_2\text{O}_{39}$.

The temperature function of heat capacity of $\text{Bi}_{24}\text{Co}_2\text{O}_{39}$ in the temperature region from 298 K to 1000 K can be expressed as $C_{pm} = [(1467.87 \pm 47.58) + (0.29941 \pm 0.09232) T - (15888378 \pm 1861508) T^{-2}] \text{ J K}^{-1}\text{mol}^{-1}$.

The high temperature fit was compared to Neumann-Kopp rule (NKR) based on the constituent oxides,

$$C_p(\text{Bi}_{24}\text{Co}_2\text{O}_{39}) = 12 \cdot C_p(\text{Bi}_2\text{O}_3) + C_p(\text{Co}_3\text{O}_4) - C_p(\text{CoO}) \quad (3)$$

where only the nonmagnetic contribution of $C_p(\text{Co}_3\text{O}_4)$ was considered. The values of the heat capacity of binary oxides were taken from the *FactSage* database.

Based on these results, XRD, Rietveld calculations, TG and DTA analysis, and on *FactSage* calculations the relevant part of Bi-Co-O phase diagram involving the homogeneity range of $\text{Bi}_{24+x}\text{Co}_{2-x}\text{O}_{39}$ was constructed for $p_{\text{O}_2}/p^0 = 0.21$ ($p^0 = 101.3 \text{ kPa}$). The comparison of the calculated phase stability lines with the experimental DTA effects (see Figure 5) shows a satisfactory agreement. According to the available experimental data and the thermodynamic model fairly reproducing the observed homogeneity range, the sillenite phase exhibits a congruent melting at $x \sim 0.25$ and $T_{\text{cm}} = 1045 \text{ K}$ with both eutectic temperatures lying only a few Kelvin below the congruent melting point.

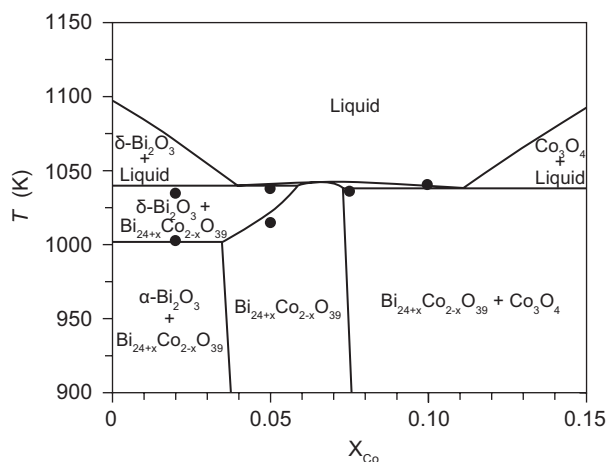


Figure 5. Phase diagram section of Bi-Co-O system in air atmosphere ($p_{\text{O}_2}/p^0 = 0.21$, where $p^0 = 101.3 \text{ kPa}$)

CONCLUSION

The $\text{Bi}_{24+x}\text{Co}_{2-x}\text{O}_{39-\delta}$ reveals a relatively wide homogeneity range from $x = 0$ to $x = 1$ and a variable oxygen content δ indicating an oxidation state of Co^{3+} at low

temperatures and a mixed state $\text{Co}^{3+}/\text{Co}^{2+}$ just below the melting temperature. However, this variation was neglected in the thermodynamic model and cobalt was considered as Co^{3+} in the sillenite solid solution and as Co^{3+} in the oxide melt. Despite this approximation the constructed phase diagram reproduces the observed thermodynamic behavior in air atmosphere. Moreover, the applied model makes it possible to predict the sillenite phase stability in a limited range of p_{O_2}/p^0 , e.g. in pure oxygen atmosphere. The measured heat capacity of the $\text{Bi}_{24}\text{Co}_2\text{O}_{39}$ end-member, although not very different from that estimated by NKR, makes the used thermodynamic model more accurate.

Acknowledgement

This work was supported by Czech Science Foundation, grant number 13-17538S and by Ministry of Education of the Czech Republic, grant number 20/2013 for specific university research.

References

1. Harwig H.A.: *Z. Anorg. Allg. Chem.* **444**, 151 (1978).
2. Vanderah T.A., Siegrist T., Lufaso M.W., Yeager M.C., Roth R.S., Nino J.C., Yates S.: *Eur. J. Inorg. Chem.* **2006**, 4908 (2006).
3. Sillen L.G., *Arkiv. Kemi.: Mineral. Geol.* **12A**, 1 (1937).
4. Valant M., Suvorov D.: *Chem. Mater.* **14**, 3471 (2002).
5. Mary T.A., Mackay R., Nguyen P., Sleight A.W.: *Eur. J. Solid. State. Inorg. Chem.* **33**, 285 (1996).
6. Belik A.A., Iikubo S., Kodama K., Igawa N., Shamoto S., Niitaka S., Azuma M., Shimakawa Y., Takano M., Izumi F., Takayama-Muromachi E.: *Chem. Mat.* **18**, 798 (2006).
7. Bale C., Chartrand P., Degterov S., Eriksson G., Hack K., Mahfoud R.B., Melancon J., Pelton A.D., Petersen S.: *Calphad* **26**, 189 (2002).
8. Tarascon J.M., Ramesh R., Barboux P., Hedge M.S., Hull G.W., Greene L.H., Giroud M., Lepage Y., McKinnon W.R., Waszczak J.V., Schneemeyer L.F.: *Solid State Commun.* **71**, 663 (1989).
9. Leligny H., Grebille D., Perez O., Masset A.C., Hervieu M., Raveau B.: *Acta Crystallogr. Sect. B-Struct. Sci.* **56**, 173 (2000).
10. Jankovsky O., Sedmidubsky D., Sofer Z., Simek P., Hejtmanek J.: *Ceram-Silikaty* **56**, 139 (2012).
11. Leitner J., Sedmidubsky D., Ruzicka K., Svoboda P.: *Thermochim. Acta* **531**, 60 (2012).
12. Arblaster J.W.: *Platinum Met. Rev.* **38**, 119 (1994).
13. Jankovský O., Sedmidubský D., Sofer Z.: *J. Eur. Ceram. Soc.* **33**, 2699 (2013).